Applied Energy 360 (2024) 122786

Contents lists available at ScienceDirect

Applied Energy

journal homepage: www.elsevier.com/locate/apenergy

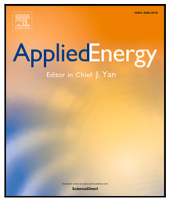

GEMSToolbox: A novel modelling tool for rapid screening of mines for geothermal heat extraction

Julien Mouli-Castillo [a,b,*], Jeroen van Hunen [b], Michael MacKenzie [b], Thomas Sear [b], Charlotte Adams [c]

[a] James Watt School of Engineering, University of Glasgow, James Watt South Building, G12 8QQ, Glasgow, UK
[b] Department of Earth Sciences, Durham University, Science Labs, Lower Mountjoy, South Rd, Durham, DH1 3LE, UK
[c] The Coal Authority, 200 Lichfield Ln, NG18 4RG, Mansfield, UK

ARTICLE INFO

Dataset link: https://github.com/JulienMC/GEMSToolbox_v1/tree/main

Keywords:
Geothermal
Renewable heat
Mine water
Modelling

ABSTRACT

Mine water geothermal heat extraction is a promising technology to provide long-term, zero carbon heating in former coal mining regions. However to allow the technology to develop further, modelling tools which are faster than 3D coupled-process simulators and more site specific than analytical solutions need to be developed. A novel modelling tool, *GEMSToolbox*, was designed for assessing the feasibility of disused and flooded mine workings for such geothermal heat extraction. The basis of *GEMSToolbox* is built upon tested, computationally efficient modelling methods, and combines efficient solvers for water flow through the mine workings with fast solution methods for heat exchange between the water in the mine galleries and the surrounding rock mass. It expands and improves on these methods by (1) allowing for arbitrarily complex multi-seam mine geometries, and (2) addressing potential thermal interaction between nearby mine galleries using a novel geometric weighting technique. Fast calculation allows for wide parameter investigation studies that is required given the often uncertain state of disused mine systems. This makes the tool ideally suitable for the feasibility stage of a project for which site-specific yet computationally efficient alternative tools are currently lacking. The tool is demonstrated on a case study using plans from a real mine system and shows how it can be used to evaluate the long-term thermal performance of a mine water geothermal heat scheme.

1. Introduction

Natural gas consumption and its associated CO_2 emissions have increased by 14% globally between 2016 and 2021 [1]. Natural gas usage has risen in the United Kingdom, owing to an increased reliance on natural gas for residential heating, which currently serves roughly 74% of households [2]. As a result, the residential use of gaseous fuels for heat accounts for 52% of UK energy consumption [3–5], and is responsible for 14% of the UK's CO_2 emissions in 2022 [6].

Therefore, it is critical to create a new approach to provide society with carbon-free, affordable, geo-politically secure, and dependable heat. In the UK, the government has the ambition that natural gas boilers will be phased out in new homes around 2035. These measures are aimed at preparing the UK for net zero carbon emission by 2050 [7].

One of the proposed low-carbon heat resources is mine water geothermal heat (MWGH) extraction. As a legacy from its prominent coal mining history, the UK has around 23,000 mines [8], and most of these are disused and flooded today. Mine temperatures in the UK follow a typical thermal gradient of 28 °C/km within a few hundred meters depth from the surface [9], and therefore the water in those mines has a typical temperature between 12–20 °C [8], depending on the depth of the mine system. Using heat pump technology to boost temperatures, the heat from this mine water can be transferred into a closed-loop system that provides heat to the end users via a heat network [10,11]. The very large volume of water residing in those disused mines, and the proximity of these mines to many residential areas (it is estimated that one in four homes or businesses is located near one of these mines), make MWGH a potentially very substantial heat resource [3].

Similar opportunities exist in active coal mining regions like China [12] where the development of mine water heating is proposed concurrently with the production of mineral resources and as a way to increase the value of backfilled areas of the mine [13,14]. The nature of these developments however, offer much easier planning and access opportunities to the mine workings which should reduce the need for scoping tools like *GEMSToolbox*, which is much more applicable to disused mines with limited access.

* Corresponding author at: James Watt School of Engineering, University of Glasgow, James Watt South Building, G12 8QQ, Glasgow, UK.
E-mail address: julien.mouli-castillo@glasgow.ac.uk (J. Mouli-Castillo).

https://doi.org/10.1016/j.apenergy.2024.122786
Received 21 August 2023; Received in revised form 18 January 2024; Accepted 30 January 2024
Available online 10 February 2024

Nomenclature

A	Cross-sectional area of flow (m^2)
$\mathbf{A}_{10}$	The subset of $\mathbf{A}_{120}$ for nodes of known hydraulic head (–)
$\mathbf{A}_{11}$	Diagonal matrix whose generic term $\mathbf{A}_{11}(k,k) = l_k\lvert Q_k\rvert^{\alpha_k-1}$ ($m^{-2}\cdot s$)
$\mathbf{A}_{12}$	The subset of $\mathbf{A}_{120}$ for nodes of unknown hydraulic head (–)
$\mathbf{A}_{120}$	Connectivity matrix of the pipe network of size $[p; N]$ (–)
b	Half thickness of the goaf area (m)
c_r	Rock specific heat capacity ($J\cdot kg^{-1}\cdot K^{-1}$)
c_w	Water specific heat capacity ($J\cdot kg^{-1}\cdot K^{-1}$)
COP	Coefficient of Performance of the heat pump (–)
D	Pipe internal diameter (m)
$\mathbf{D}_{11}$	Diagonal matrix of the derivatives of $\mathbf{A}_{11}$ with respect to $\mathbf{Q}$ ($m^{-2}\cdot s$)
f	Darcy friction factor (–)
g	Acceleration due to gravity ($m\cdot s^{-2}$)
h	Heat transfer coefficient ($W\cdot m^{-2}\cdot K^{-1}$)
$\mathbf{H_0}$	Vector of known nodal heads (m)
$\mathbf{H}$	Vector of unknown nodal heads (m)
H_D	The heat demand for van Mildert College accommodation (J)
H_i	Hydraulic head value at node i (m)
H_j	Hydraulic head value at node j (m)
l	Loss constant in the head loss equation ($m^{-5}\cdot s^2$)
L	The length of a pipe (m)
m	Mass of water flowing through the pipe during a period t (kg)
n_i	The number of pipes connected to node i (–)
Nu	The Nusselt number (–)
P	Effective perimeter perpendicular to the flow direction (m)
Pr	Prandtl Number (–)
$\mathbf{Q}$	Vector of unknown pipe discharges ($m^3\cdot s^{-1}$)
$\mathbf{Q_d}$	Vector of nodal demands ($m^3\cdot s^{-1}$)
Q_{abs}	The abstraction flow rate for the Van Mildert Case Study ($m^3\cdot s^{-1}$)
Q_{d_i}	The known nodal demand at node i ($m^3\cdot s^{-1}$)
Q_H	Amount of heat transferred to the water from the rock (J)
Q_k	The volumetric flow rate through pipe k ($m^3\cdot s^{-1}$)
$Q_{k_{ij}}$	The volumetric flow rate through pipe k linking node i to j ($m^3\cdot s^{-1}$)
q_p	The heat flux through the gallery wall ($W\cdot m^{-2}$)
r_0	Radius of the effective thermal 'halo' around the pipe (m)
r_p	The radius of the pipe equal to $D/2$ (m)
Re	The Reynolds number (–)
T	Temperature (°C)
t	Time (s)
T_{in}	Water temperature at entrance of the pipe (°C)
T_{out}	Water temperature at exit of the pipe (°C)
T_p	The temperature of the pipe wall (°C)
T_r	Initial rock mass temperature (°C)
T_w	The mean temperature of the water within the pipe (°C)
v_w	Water average linear velocity ($m\cdot s^{-1}$)
α	Darcy–Weisbach exponent (–)
ΔT_{HX}	Temperature difference across the heat pump's mine water heat exchanger (°C)
ΔT_{mp}	Water temperature change along the pipe predicted by the planar model (°C)
ΔT_{mr}	Water temperature change along the pipe predicted by the radial model (°C)
ϵ	Darcy–Weisbach roughness coefficient of the pipe internal walls (m)
η	Weighting factor for the temperature models (–)
λ_r	Rock thermal conductivity ($W\cdot m^{-1}\cdot K^{-1}$)
λ_w	Water thermal conductivity ($W\cdot m^{-1}\cdot K^{-1}$)
μ_w	The dynamic water viscosity ($N\cdot s\cdot m^{-2}$)
μ_{th}	Thermal performance of the mine water system (–)
Φ	Function describing the friction-induced head loss through open pipes (m)
ρ_r	Rock density ($kg\cdot m^{-3}$)
ρ_w	Water density ($kg\cdot m^{-3}$)
τ	Current iteration in the Newton–Raphson iteration scheme (–)
θ	Angle used for integration of η (radians)
Y	Total heat transfer coefficient ($W\cdot m^{-2}\cdot K^{-1}$)

But MWGH extraction also has a number of challenges [15]. There are environmental issues to address when abstracting mine water, due to its potential acidity, salinity, and high concentration of metals and sulfides. To avoid environmental contamination, careful planning and application for abstraction, discharge, and/or reinjection of the mine water will be needed. Unless the mine system is already pumped into a water treatment site, surface discharge is unlikely to be licensed, and reinjection of the minewater will be necessary. Unless air/oxygen is excluded from the system, oxidation of iron during abstraction may form ochre, and clog the pipe network, leading to higher maintenance costs and operational difficulties. Despite these challenges recent research estimates that the Scottish Coalfields could produce up to 48 MW of heat and should be co-developed with heat networks [16]. In addition, several logistical challenges exist. A number of mine water heat abstraction schemes have been deployed [17], depending on the local situation. In some cases, shafts remained accessible after mining operations ceased, but more often they were sealed and are now unsuitable for accessing the mines. Therefore, boreholes may need to be drilled to access the mine water, which adds significantly to the capital costs of any MWGH project.

So the most common method for extracting mine water heat will be through an open-loop system, in which mine water is pumped up through an existing shaft or a purpose-drilled borehole, some of its heat extracted, and the cooler water re-injected into a different part of the mine system [15]. This will set up a circulation, with flow inside the mine system, in which the cold, reinjected water will gradually warm up while flowing towards the extraction point again.

A number of such open-loop mine water heat extraction schemes have been successfully applied, including in Heerlen, the Netherlands, in Asturias, Spain, and in Gateshead, UK (see [17] for a recent overview). The geometries of the mine roadways have significant uncertainties due to simplified, inaccurate, or incomplete mine maps, or potential modifications of the mine after closure, e.g. a local collapse. The effectiveness and longevity of the heat extraction process is therefore difficult to predict, and modelling of the open-loop system is sometimes used to assess the feasibility of a mine system for heat

extraction, for example in Heerlen which has been in operation for over a decade [18]. At other times, volumetric estimates are performed to assess the resource available. This usually involves estimating the mine water volume available and its temperature to estimate how much heat is available. This approach is over-simplistic and carries significant risks as it does not take into account the efficiency with which the mine water can be extracted as will be shown later in the results. The uncertainty associated with the pre-drilling phase of mine water project, and the potential for heat depletion over the lifetime of the project, have been highlighted as two of main barriers to the development of the technology [8]. Some of the partners on the Geothermal Energy from Mines and Solar Geothermal Heat (GEMS) project have also expressed the need for this type of tools to inform regulation and business cases. To address these uncertainties and quantify these risks new modelling tools are needed.

Most mechanistic modelling methodologies to date fall within two distinct categories, either that of numerical codes [18–22], or analytical models. These methodologies have been extensively reviewed in [23] and the reader is referred to this work for an in depth discussion on the pros and cons of each approach. A few recent studies published since that review are discussed below. Numerical approaches tend to be computationally expensive as they attempt to couple fluid flow and heat transport (and sometimes more processes) to a real site [18]. The following numerical approaches have been used to model mine water heating systems: Finite Difference Method (FDM), Finite Element Method (FDM) and the Finite Volume Method (FVM). MODFLOW developed by the US Geological Survey, SHEMAT [24] and TOUGH2 [25] offer an FDM implementation, whilst alternatives like FEFLOW, COMSOL Multiphysics and OpenGeoSys [26] offer FEM packages suitable for handling more complex geometries. ANSYS' Fluent, and MARTHE [27] are FVM alternatives to the approaches above. It is important to recognise that employing such codes to achieve a complete and intricate representation of geometry is exceedingly challenging due to the substantial computational resources demanded and the proliferation of numerical instabilities [18]. To palliate to this issue, others focus on conceptual process understanding without explicitly modelling real sites and their complexity [19,20,22]. For example, Bao and Liu [22] investigate detailed stratification patterns in mine water shafts. These works focus on presenting new concepts and building understanding of underlying processes, rather than modelling specific sites to the level required for a feasibility study. Another approach uses analytical models, such as offered by [28], which are much faster and scalable. But these solutions quickly run into limitations due to the often oversimplified assumptions (e.g. homogeneous rock mass, isolated galleries) which break down when applied to real sites.

Modelling offers a cost-effective tool to assess the viability of mine workings for mine water heating before deployment of expensive infrastructure is commenced. The uncertainty of the state of the mines requires a fast modelling tool that can quickly evaluate a wide range of scenarios, and analytical solutions are ideal for that. But the structural complexity of mine workings requires a versatile modelling tool that can assess elaborate, varied and composite mine settings, which, so far, only computationally expensive, fully numerical tools can offer. Hence, there is a need for a flexible modelling tool which can be used in the early phases of mine water project feasibility studies to provide insights on a project's viability that analytical or complex 3D numerical models cannot offer at this project stage. Such tool can also be used to provide functions describing the performance and constraints of the subsurface system which could be used for to optimise the integration of specific mine workings to the wider energy system using approaches similar to [29].

To fill that gap in mine water project feasibility assessments, we provide a novel modelling tool called *GEMSToolbox* that can be easily and quickly applied to assess the feasibility of a mine system for MWGH extraction, and explore optimal injection and abstraction flow rates and site locations. It contributes to filling the gap in applying theory to real projects by providing fast computations on a detailed geometry. In the following sections, we provide a mathematical and numerical description of the *GEMSToolbox*, provide the various validation techniques for the code, and illustrate the potential of this tool through application to a real-case scenario.

2. Method

2.1. Principles and conceptual model

The heat extraction scheme considered here is an open loop system [15]. Given the uncertainties associated with the state of flooded mine systems, detailed, high-resolution models are unlikely to provide more insight than models that capture the first-order features only [30]. To establish the flow of water through the mine system, a network of mine galleries is therefore effectively modelled as a network of connected pipes (Fig. 1). The crossroads are represented as nodal points and the connecting galleries as cylindrical pipes, following the approach detailed for the US Environmental Protection Agency tool EPANET2 [31]. The injection and extraction of water at a given rate and given locations in the mine system creates a hydraulic pressure gradient that induces a flow that matches the rates of injection and extraction at the wells [31,32]. Conceptually, the open galleries offer orders of magnitude less resistance to flow than the surrounding rock mass dominated by slower fracture and porous flow. Therefore, we assume that the mines do not exchange much water with the surrounding rock mass. Furthermore, we consider an open loop system, where as much water is injected as abstracted from connected mine workings.

As the water flows through the mine system, heat exchange takes place between the water and the surrounding rock formations, wherever a temperature difference exists between the flowing water and the rock temperature [30]. In turn, this leads to a temperature gradient developing inside the rock over time. In the context of mines densely excavated using a 'room and pillar' method, this temperature gradient may result in thermal interference between neighbouring galleries in the plane of the coal seam, particularly over longer time scales. Since this work is primarily concerned with the lifetime assessment of these mines for geothermal use, we expect this thermal interference to be significant, and account for it in this modelling as described subsequently.

2.2. Hydraulic model

2.2.1. Mathematical model

The hydraulic model used is described in [33]. The reader is referred to their work for more detail.

The fundamental equations which describe the hydraulic head distribution and flow of water through a water distribution network, and applied here to mine workings with open pipes, are the conservation of energy, and the conservation of mass.

Conservation of energy. The conservation of energy is described by Bernoulli's principle applied to the length of each pipe k in the network.

$$H_i - H_j - \Phi(Q_k) = 0, \tag{1}$$

where H are the hydraulic heads at nodes i and j at either end of pipe k. $\Phi(Q_k)$ describes the friction induced head loss across pipe k between those nodes, as a function of the flow Q_k through that pipe.

Fig. 1. Left hand side showing an original mine plan from the UK's Coal Authority. The dimensions are about 500 by 500 m. The right hand side shows the result of the digitisation of the mine plan using GIS.
Source: Reproduced with the permission of © The Coal Authority. All rights reserved

Conservation of mass. Conservation of mass requires that there is no net in- or outflow of water at each node in the network:

$$\sum_{k=1}^{n_i} Q_k + Q_{d_i} = 0, \tag{2}$$

where Q_k is the flow through each of the n_i pipes connected to node i, and Q_{d_i} is the known demand (or injection/abstraction rate) at node i. The flow convention we use is that flow into a node is positive and the outflow is negative.

As described in [33], the head loss function across a pipe Φ is expressed as a power function of the flow Q_k through that pipe k

$$\Phi = l_k |Q_k|^{\alpha-1} Q_k \tag{3}$$

where α is an exponent with a value of 2 when using the Darcy–Weisbach equation. l_k is a coefficient that depends on the pipe's diameter, length and flow rate

$$l = \frac{8 f L}{\pi^2 \, g D^5}, \tag{4}$$

where D is the pipe diameter (m), L the pipe length (m), and g the acceleration due to gravity ($m \cdot s^{-2}$). To calculate the Darcy friction factor f, we first need to determine if the flow through the segment is laminar or turbulent [34], using the Reynolds number, Re:

$$Re = \frac{\rho_w v_w D}{\mu} \tag{5}$$

in which ρ_w and μ are the density and dynamic viscosity of the fluid, respectively, and $v_w = \frac{4Q}{\pi D^2}$ the fluid velocity. For $Re < 2000$, the flow is considered laminar, and the friction factor can be determined using [34]:

$$f = \frac{64}{Re} \tag{6}$$

For $Re > 4000$, the flow is considered turbulent, and the Swamee–Jain approximation to the Colebrook-White equation was used [31,35]:

$$f = \frac{0.25}{\left[\log_{10}\left(\frac{\epsilon}{3.7D} + \frac{5.74}{Re}\right)\right]^2} \tag{7}$$

where ϵ is the Darcy–Weisbach roughness coefficient. For intermediate Reynolds number values 2000 <= Re <= 4000, a cubic interpolation is used, see Appendix D of [31] p. 189 and original derivation in [36].

Substituting Eq. (3) into Eq. (1) gives:

$$H_i - H_j - l_k |Q_k|^{\alpha-1} Q_k = 0 \tag{8}$$

Eqs. (2) and (8) form the governing equations of a generic water distribution network. Provided that the mine workings are open galleries, these equations are applicable to model the flow of water through such systems. Note that this approach implies that we ignore any localised friction induced by obstacles in the galleries, as well as interaction with the groundwater seeping in and out of the surrounding country rock.

2.2.2. Hydraulic head and flow computation

To solve this system of equations, we follow [33].

We first describe the connectivity of all p mine galleries (or pipes) with all N intersections (or nodes) by an incidence matrix $\mathbf{A_{120}}$ of size $[p; N]$ relating the pipes to the nodes as follows:

$$\mathbf{A_{120}} = \begin{cases} -1, & \text{if pipe } i \text{ leaves node } j \\ 0, & \text{if pipe } i \text{ is not connected to node } j \\ +1, & \text{if pipe } i \text{ enters node } j \end{cases} \tag{9}$$

We then separate $\mathbf{A_{120}}$ into two matrices $\mathbf{A_{12}}$ and $\mathbf{A_{10}}$,

$$\mathbf{A_{120}} = [\mathbf{A_{12}} \; \mathbf{A_{10}}] \tag{10}$$

with matrix $\mathbf{A_{12}}$ of size $[p; nn]$ describing the connectivity for the nn nodes with an unknown hydraulic head, and a matrix $\mathbf{A_{10}}$ of size $[p; no]$ for the no nodes with a fixed hydraulic head. We refer to the transpose of $\mathbf{A_{12}}$ and $\mathbf{A_{10}}$ as $\mathbf{A_{21}}$ and $\mathbf{A_{01}}$, respectively. Furthermore, part of Eq. (3) is defined as:

$$\mathbf{A_{11}}(k,k) = l_k |Q_k|^{\alpha-1} \tag{11}$$

We can then combine Eqs. (2) and (8) in matrix notation as in [32]:

$$\begin{bmatrix} \mathbf{A_{11}} & \mathbf{A_{12}} \\ \mathbf{A_{21}} & 0 \end{bmatrix} \begin{bmatrix} \mathbf{Q} \\ \mathbf{H} \end{bmatrix} = \begin{bmatrix} -\mathbf{A_{10}} \mathbf{H_0} \\ -\mathbf{Q_d} \end{bmatrix} \tag{12}$$

with:

$\mathbf{Q} = [Q_1, Q_2, \ldots, Q_p]^T$, the unknown pipe discharges vector of size [1, p],

$\mathbf{H} = [H_1, H_2, \ldots, H_{nn}]^T$, the unknown node hydraulic heads vector of size [1, nn],

$\mathbf{H_0} = [H_{nn+1}, H_{nn+2}, \ldots, H_{nn+no}]^T$, the known node hydraulic heads vector of size [1, no], and

$\mathbf{Q_d} = [Q_{d_1}, Q_{d_2}, \ldots, Q_{d_{nn}}]^T$, the node demands vector of size [1, nn]. This formulation produces a set of $p + nn$ unknowns.

Eq. (12) is solved using a Newton–Raphson (NR) iterative approach [32,33]. In practice, the following [*nn*; *nn*] system of equations is solved for $\mathbf{H}^{\tau+1}$ [33]:

$$[\mathbf{A_{21}}(\mathbf{D_{11}^{\tau}})^{-1}\mathbf{A_{12}}]\mathbf{H}^{\tau+1} = \mathbf{A_{21}}(\mathbf{D_{11}^{\tau}})^{-1}[(\mathbf{D_{11}^{\tau}} - \mathbf{A_{11}^{\tau}})\mathbf{Q}^{\tau} - \mathbf{A_{10}}\mathbf{H_0}] + \mathbf{Q_d} \quad (13)$$

where $\mathbf{D_{11}}$ is the derivative of $\mathbf{A_{11}}$ with respect to $\mathbf{Q}$, as described in Appendix B. $\mathbf{D_{11}^{\tau}}$ is $\mathbf{D_{11}}$ evaluated for the flows $\mathbf{Q}^{\tau}$ at the current iteration τ.

The flow is then updated using:

$$\mathbf{Q}^{\tau+1} = \mathbf{Q}^{\tau} - (\mathbf{D_{11}^{\tau}})^{-1}(\mathbf{A_{11}^{\tau}}\mathbf{Q}^{\tau} + \mathbf{A_{12}}\mathbf{H}^{\tau+1} + \mathbf{A_{10}}\mathbf{H_0}) \quad (14)$$

2.3. Heat exchange model

As water flows through the galleries (or pipes) from the injection point to the abstraction point, its temperature at each node is calculated as the flow-weighted average of the water from all galleries feeding the node with water. Galleries downstream of this node will be fed with water with this average temperature. Here we first present the processes considered for the heat transfer between the water in the mine galleries and the surrounding rock mass. Next we describe the thermal model to account for the thermal interference which develops between galleries over time.

2.3.1. Theory of heat transfer between rock mass and gallery

Three main quantities are required to compute the change in temperature of the water as it flows through a gallery: the heat flow through the rock, the heat flow from the rock to the water, and, the resulting temperature change.

Heat flow in the rock mass. The heat diffusion process is expressed by Fourier's law which leads to the following conservation of thermal energy equation:

$$\rho_r c_r \frac{\partial T}{\partial t} = -\nabla(-\lambda_r \nabla T) \quad (15)$$

where λ_r is the thermal conductivity of the rock, ρ_r its density, and c_r its specific heat capacity.

Heat exchange between rock mass and water. Heat transfer between the rock and the water is calculated for each gallery separately, and is derived from the difference between the gallery wall temperature and the mean water temperature flowing through the gallery:

$$q_p = h(T_p - T_w) \quad (16)$$

where q_p is the heat flux through the gallery wall in $\mathrm{W \cdot m^{-2}}$, T_p is the gallery wall temperature and T_w is the mean temperature of water within the gallery, and the heat transfer coefficient h is given by:

$$h = \frac{\lambda_w Nu}{D} \quad (17)$$

with λ_w the thermal conductivity of the water in $\mathrm{W \cdot m^{-1}K^{-1}}$, and Nu the Nusselt number, and D the pipe diameter. The Nusselt number is defined using different empirical relationships depending on the fluid and heat flow regimes defined by the Reynolds number (Eq. (5)) and Prandtl number Pr:

$$Pr = \frac{c_w \mu_w}{\lambda_w} \quad (18)$$

where c_w is the specific heat of water in the pipe, and μ_w the dynamic viscosity of the water in $\mathrm{N \cdot s \cdot m^{-2}}$.

If $3000 \leq Re \leq 5 \times 10^6$ and $0.5 \leq Pr \leq 2000$, Nu is defined using the Gnielinski correlation [37]:

$$Nu = \frac{(f/8)(Re - 1000)Pr}{1 + 12.7 * (f/8)^{1/2}(Pr^{2/3} - 1)} \quad (19)$$

where f is the Darcy friction factor defined previously. It should be noted that the transition from laminar to turbulent flow is dependent on multiple parameters and that each individual correlation has been developed for a particular set of conditions. However, these difference are minor relative to the geological uncertainties present in these systems.

If the flow regime is laminar the Hausen Equation is applied [38]. The applicability criteria is: $Re \leq 3000$ and $Pr \geq 5$.

$$Nu = \frac{3.66 + (0.0688(D/L)RePr)}{1 + 0.04((D/L)RePr)^{2/3}} \quad (20)$$

where, D is the pipe diameter (m), and L the pipe length (m).

In all other cases the simplified Dittus-Boelter Equation is applied, similar to that used in [30]:

$$Nu = 0.021 Re^{0.8} Pr^{0.43} \quad (21)$$

In practice, however, for mine geometries and flow rates used in commercial schemes (10 s to 100 s of L/s), Eq. (21) is rarely needed.

Heat flow within the gallery. The change in water temperature ΔT as it flows through the gallery over a period of time t is obtained by first estimating the total heat transfer from the rock to the water over that time period:

$$Q_H = \pi D L q_p t \quad (22)$$

where D is the diameter of the gallery, L its length, and q_p the heat flux through the gallery walls. The temperature change is then estimated as:

$$\Delta T = Q_H/(mc_w) \quad (23)$$

where m is the mass of water (in kg) that is flowing through the pipe over the period t. It is assumed that the fluid and rock properties other than temperature are constant for each gallery.

2.3.2. Analytical models

Several analytical (or semi-analytical) solutions for heat transfer are presented here, and used in the applied heat exchange model in Section 2.3.3.

Analytical cylindrical heat transfer model. Radial heat exchange between a homogeneous rock mass of uniform temperature T_r surrounding a cylinder and water inside the cylindrical gallery is derived semi-analytically using the method originally developed by Rodríguez and Díaz [30]. The temperature at the end of the gallery $T_{out,mr}$ can be obtained from:

$$T_{out,mr} = \frac{2\pi r_p L Y T_r + (\rho_w c_w Q - \pi r_p L Y)T_{in}}{\rho_w c_w Q - \pi r_p L Y} \quad (24)$$

where Y is defined as the effective heat transfer coefficient of the combined rock and water system:

$$Y = \frac{1}{\frac{1}{h} + \frac{r_p}{\lambda_r}\ln\left(\frac{r_0}{r_p}\right)} \quad (25)$$

with r_p the pipe internal radius (m), L the pipe length (m), T_r the initial rock temperature (°C), ρ_w the water density ($\mathrm{kg.m^3}$), c_w the water specific heat capacity ($\mathrm{J \cdot kg^{-1} \cdot K^{-1}}$), Q the flow rate through the pipe ($\mathrm{m^3 \cdot s^{-1}}$), T_{in} the water temperature at the start of the pipe, and r_0 the effective thermal 'halo' around the pipe, further elaborated on below and in Appendix A. A few modifications were applied to the original formulation of Rodríguez and Díaz [30]. Firstly, as recommended by Loredo et al. [38], the heat transfer coefficient Eq. (17) is refined using one of the Nusselt numbers from Eqs. (19) or (20), depending on the flow regime inside the gallery. Secondly, the original calculation of the heat loss from the rock mass (their Eq. (A.12)) is refined. Thirdly, the calculation of the gallery wall temperature T_p and thermal 'halo' parameter r_0 is improved by removing the assumption that T_p should be the average of the water and original rock temperatures. The rationale and full derivation of the new T_p and r_0 are provided in Appendix A.

Analytical planar heat transfer model. The temperature change of a fluid moving along a fracture plane due to heat exchange with and diffusion through the rock mass surrounding the fracture can be determined analytically [28,39]. The formulation can be adapted to a cylindrical pipe by expressing the surface area of the pipe as a planar heat surface on which the heat transfer occurs [38]. The temperature change of the fluid at a distance L within a generalised flow channel from the point of injection is given by:

$$T_{out,mp} - T_r = \Delta T_1 = (T_{in} - T_r)\mathrm{erfc}(\Psi)U(\xi - \zeta) \tag{26}$$

where

$$\Psi = \frac{LP}{2qc_w}\sqrt{\frac{\lambda_r \rho_r c_r}{t - \frac{LA\rho_w}{q}}} \tag{27}$$

$$\zeta = \frac{L\lambda_r}{r_p^2 \rho_w c_w v_w} \tag{28}$$

$$\xi = \frac{t\lambda_r}{r_p^2 \rho_w c_w} \tag{29}$$

and where T_r is the initial rock mass temperature (°C), U is equal to 1 if $\xi - \zeta$ is positive and 0 if not, T_{in} the temperature of the injected water (°C), $T_{out,mp}$ the temperature (°C) at distance (m) L from the inflow point, P the effective perimeter (m) perpendicular to the flow direction, and A its surface area (m^2), λ thermal conductivity ($W \cdot m^{-1} \cdot K^{-1}$), ρ density ($kg \cdot m^3$), c specific heat capacity ($J \cdot kg^{-1} \cdot K^{-1}$), r_p the radius of the pipe (m) for any generalised flow void (in this case the mine gallery), and where the subscripts r and w stand for the rock and water respectively.

2.3.3. Temperature and heat transport computation in GEMSToolbox

Determining order of computation. Heat transport is calculated from any inflow points in the system to any outflow points. To increase efficiency, first, a tree structure of nodes in the order in which they are to be solved is built, using the flow field from Section 2.2.2. How this tree is built is described in detail in Appendix B.

Accounting for thermal interference between galleries. The radially symmetric approach from [30] assumes that heat is available from an unlimited rock mass surrounding the galleries, and the distance from which heat is extracted (or the 'thermal halo') is represented by an ever-increasing radius r_0. In reality, a thermal interference is likely to occur between nearby galleries, when, for long-term heat extraction, the thermal halo from one gallery starts to overlap with that of a neighbouring gallery. Here, an efficient model to deal with this thermal interference is proposed by computing the temperature exchange using both the radial and planar models described in Section 2.3.2.

Due to this thermal interference, each gallery is only able to extract heat from its own 'control volume' surrounding the gallery, which is smaller if galleries are positioned closer together (Fig. 2A). In the plane perpendicular to the axis of the gallery, let r_{min} be the minimum distance from the gallery axis to the edge of the control volume. As long as $r_0 \leq r_{min}$, the radially symmetric heat extraction assumption from [30] remains valid. For $r_0 > r_{min}$, thermal interference between the gallery and its neighbour starts to occur. For $r_0 \gg r_{min}$, heat extraction in the plane of the galleries (i.e. the coal seam) becomes negligible, and heat extraction approaches a planar model, in which heat is only extracted from the direction perpendicular to the coal seam (i.e. typically vertically above and below a horizontal coal seam). In *GEMSToolbox*, the heat extraction is approximated as a weighted average of a radial and a planar model presented earlier in Section 2.3.2. In the plane perpendicular to the axis of the gallery, let $r(\theta)$ be either r_0 or the distance from the gallery centre to the edge of the control volume in the direction θ, whichever of the two distances is smaller (see red line in Fig. 2B and blue line in Fig. 2C). The proportion of radial versus planar heat diffusion applied, here referred to as the weighing factor η, is then defined as:

$$\eta = \frac{\int_{\theta=0}^{2\pi}(r(\theta) - r_p)d\theta}{2\pi(r_0 - r_p)} \tag{30}$$

The temperature change of the water ΔT flowing through the gallery is then defined as a linear combination of the radial and planar solution Eqs. (24) and (26):

$$\Delta T = \eta \Delta T_{out,mr} + (1 - \eta)\Delta T_{out,mp} \tag{31}$$

2.4. Model file structure

The model directory is organised in subdirectories: inputfiles, sc (source code), data, results.

The input file is a comma separated file (csv). Each file row represents a different simulation run parameters and each column a parameter. The DefaultScenario.csv contains all the default parameter values. An input file can be created either from a blank csv or by copying the default file. A user does not have to specify a value for all the parameters. Any missing parameter will be automatically read from the DefaultScenario.csv file and a warning issued to the user for reference. This arrangement has the advantage of making creating input files easy for non-programmers using MS Excel or similar. Furthermore it afford a way to easily keep a record of all the parameter values used. Finally, it makes it easy to generate large simulation sequences (simply by adding extra rows) for conducting sensitivity analysis or uncertainty quantification. A detailed description of all the parameters, including how to set boundary conditions and initial conditions is provided in the README file on GitHub. To determine which input file to run, its name should be specified in the _InputFileName.csv. To perform the simulation run the following file GEMSToolbox.m.

The results of each run can be found in the 'results' directory under a sub-directory which has the same name as the input file. Two kind of result files are generated, the first is a summary of all the well temperature given as the 'thermal performance' introduced later in this work. The second is the 3D VTK file of each simulation (i.e. each row in the input file). These files can be visualised in ParaView.

The data folder is added for convenience only. Users can specify geometry files located anywhere in practice.

2.5. Validation tests

The numerical code is thoroughly benchmarked against a set of analytical and numerical test results. The following tests were designed to verify the implementation of the flow and heat transfer calculations. All test methods and results are detailed in the Appendix C.

2.5.1. Flow validation

To validate the flow calculations, a test case was designed where 10 successive pipes are connected in series. Each pipe is a 100 m long. The pipe diameters vary between each pipe (see Appendix C Table C-1). The narrowest pipe has a diameter of 10 cm and the largest of 10 m. A fixed hydraulic head of 2 m is set at the entrance of the narrowest pipe and a fixed hydraulic head of 0 m is set at the exit of the final, widest, pipe. The results of the *GEMSToolbox* implementation were compared against the Excel implementation of Eq. (8) for each pipe (see Appendix C Table C-1).

2.5.2. Heat transfer validation

To verify the implementation of the heat transfer coefficient the results were compared to previous work. For the test, the base case from [30] at 10 and 40 $m^3 \cdot h^{-1}$ was implemented, as reported in [38] (see their Table 1 for input parameters). It should be noted that the *GEMSToolbox* approach uses their recommendation of using more representative Nusselt number relationships.

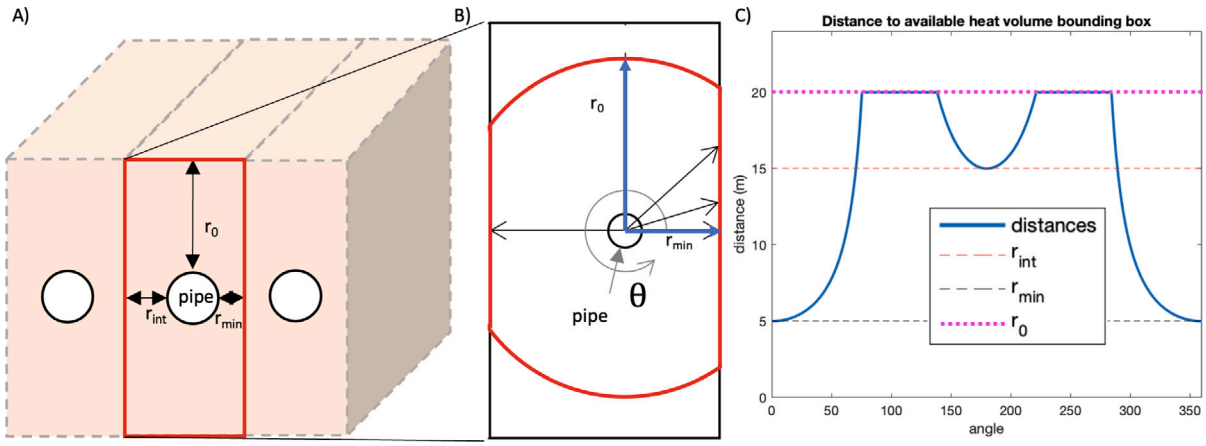

Fig. 2. (A) Representation of the volume of rock that the pipe can exchange heat with. The maximum distance is given by r_0, the closest mid-distance between two pipes by r_{min}. In a dense mine network a gallery often has two adjacent galleries. The mid-distance to the second closest gallery is r_{int}. (B) Schematic representation of the integration used to determine the thermal interference between neighbouring galleries. (C) Output of the computation of r_i (i.e. all the distances between the pipe centre and the bounding box are shown in the blue continuous line). In this example r_0 = 20 m, r_{min} = 5 m, r_{int} = 15 m.

2.5.3. Interference between mine galleries

To verify the validity of the weighting factor η, testing was conducted where the results of the *GEMSToolbox* using η were compared against the results of a full 2-D finite element solution. The details of the tests and its results are provided in the Appendix C.

2.6. Durham university case study

Next, the description of how the model is applied to a hypothetical mine-water heat abstraction scheme utilising the mine workings located beneath the Durham University Campus is provided. In this scheme, mine water is abstracted from one of the mine workings of the deeper "Busty" seam, and re-injected into the shallower "Hutton" seam. The water will then flow back from the injection point in the Hutton seam, via shafts connecting the seams to the abstraction point in the Busty seam. In this project, the scheme aims to provide the heat demands for one of the University's colleges, Van Mildert College, for which heat demands were obtained from Durham University [40]. Therefore, mine water is hypothetically injected and abstracted at the Van Mildert site using a borehole into the mine workings of each of the seams.

2.6.1. Evaluating heat demand

Durham University uses an Energy Manager software tool, Systemslink, that allows for detailed monitoring and reporting of gas and electricity data. The data from March 2020 to February 2022 is used. The data samples are available with a 30-minute interval window.

In this study two scenarios are investigated. The first assumes that the total energy demand is spread over the course of the year. The second assumes that the peak energy demand is extracted throughout the year.

For the first scenario, the total annual gas demand for the accommodation blocks of Van Mildert College amounts to 1,672,163 kWh (± 53,266 kWh), which amounts to 191 kW when the demand is spread evenly over 365 days. For the second scenario, the peak gas consumption from the seven residential blocks at the Van-Mildert College was 2156 kW. This is a theoretical maximum as the peak demand might not have occurred at the same time in each block. However, it is necessary to understand the maximum potential consumption for heat pump selection, and adding the peak loads together for this simple example analysis is suitable. It should be noted that the first scenario is only about 8.9% of the heat demand from the second one.

A heat pump will be used to transfer the heat from the pumped minewater into a clean closed-loop circuit. The total mine water extraction rate, Q_{abs}, to meet the heat demand for the scenarios described above can be computed as follows [41]:

$$Q_{abs} = \frac{H_D \left[1 - \frac{1}{COP}\right]}{\Delta T_H c_w \rho_w} \tag{32}$$

where H_D is the requested heat demand, COP the coefficient of performance of the heat pump, ΔT_H the mine water temperature drop due to heat extraction, and c_w and ρ_w the specific heat and density of the mine water. Table 1. A illustrates the required mine water extraction volume rates for each scenario.

Table 1
(A) Mine water extraction rate demands calculated for the two Van Mildert heating demand scenarios. This calculation uses a typical coefficient of performance of the heat pump used is 3.5 and a mine water temperature drop ΔT_H due to heat extraction of 5 °C. (B) Indicates the variation in thermal rock properties for the sensitivity analysis of the first scenario.

(A)	Hourly demand (kWh)	Well flow rates Q_{abs} ($m^3.s^{-1}$)
Scenario 1	191	6.48E−03
Scenario 2	2,156	7.36E−02
(B)	Thermal conductivity	Specific heat capacity
Sc 1 - base	2.6	960
Sc 1 - Sandstone	3.0	920
Sc 1 - Shale	2.2	1000

The variation in abstraction temperature due to variations in the thermal properties of the rocks surrounding the mine are also investigated. This is important as coal measures in this case study area are found in repeating lithological sequences. Therefore the roof of the mine consists of predominantly sandstone, and the floor predominantly of shale. Table 1.B indicates the rock thermal properties for the sensitivity analysis performed on the first scenario.

2.6.2. Digitising mine plans

The digitisation of the mine plans is essential to the modelling approach described in this study. The protocol used for digitisation is reported extensively in [40]. All UK mine plans are licensed by the Coal Authority. The maps are received as images and are geo-referenced in ArcGIS PRO before each gallery of the room and pillar workings is digitised (Fig. 3). Geo-referencing of the maps is done using surface features indicated on the maps such as buildings which have survived since the map was made, or old mine shafts that reach the surface and have been geo-referenced by the Coal Authority in the past.

Some mine plans show that portions of the old room and pillar workings have been completely removed as part of a subsequent mining phase. These areas of the mine almost certainly collapsed due to the

Fig. 3. Digitised mine plans showing the Busty Seam in red, the Hutton Seam in blue. The yellow star indicates the location of the Van Mildert College of Durham University. *Source:* From [40].

lack of structural supports from the pillars. Since the mines are very old (in some instances in the late 18th century), the collapsed material will subsequently have compacted and now acts as a relative barrier to the flow of water, compared to the open galleries and roadways in the mine workings.

Existing mine water heating projects often utilise multiple coal seams, where water is commonly injected in a shallower seam, and abstracted from a deeper seam [e.g., 41,42]. Therefore, another important element of the digitisation process is the identification of mine shafts that connect the abstraction and re-injection seams to ensure an effective re-circulation pattern is developed. This circulation prevents over-pressurisation of the re-injection seam and de-pressurisation of the abstraction seam. This is important to ensure that the water re-injected into the mine does not seep out to the surface or into aquifers containing drinking water. The connection between the abstraction and reinjection points would also be evaluated with pumping tests.

2.7. Thermal performance: A metric to assess the sustainability of a mine water heating system

In order to assess the sustainability of a mine water heating system over time the proposition is made to use a metric which normalises the difference in temperature between the injection and abstraction to the difference in temperature between the in-situ inital conditions of the system and the injection temperature. This 'thermal performance' η_{th} is defined as:

$$\eta_{th} = \frac{T_{abs} - T_{inj}}{T_r - T_{inj}} \tag{33}$$

A few properties of the thermal performance are provided below:

- It will be in the [0, 1] interval as long as the abstraction temperature is warmer or equal to the re-injection temperature, and cooler or equal to the initial in-situ temperature of the rock and mine water.
- It will be > 1 if the abstraction temperature exceeds the initial in-situ temperature of the rock. This is useful, to identify a system which is heating over time from a heat source that is not the injected water.
- It will be < 0 if the abstraction temperature is lower than the re-injection temperature. In effect, if heat is added to the water at the surface. Under the current assumptions, this is the opposite of what the aim of the system is. Hence, a negative thermal performance can be viewed as a state in which the system is physically unable to perform.

3. Results

3.1. Flow patterns and mine water temperature distribution for the Van Mildert case study

Figs. 4 and 5 illustrate the water temperature inside the mine workings after 30 years of operation for scenarios 1 and 2, respectively. Appendix D lists the differences between both scenarios. Water is injected into the upper seam at the location of Van Mildert college, and from there flows through the upper seam towards the shaft that connects the seams, where it flows into the lower seam. Inside the lower seam, the water makes its way back to the location under Van Mildert college, where it is pumped up again. The simulations were done on a MacBook Pro (M2 Chip, 16 GB of RAM) and took approximately 25 seconds each.

An important difference to observe is that in scenario 1 the water temperature at the top of the shaft connecting the two seams is still close to the initial rock temperature of the shallow seam after 30 years. This would imply that the cooling of the deeper seam is primarily driven by the initial temperature difference between the two seams as the water flows through the system. In scenario 2 however, the faster flow rates clearly cause the cold temperatures of the re-injected water (10 °C) to reduce the temperature at the top of the shaft below the initial rock temperature of the shallow seam. In effect, the thermal effects of the re-injection well can be felt at the shaft and hence in

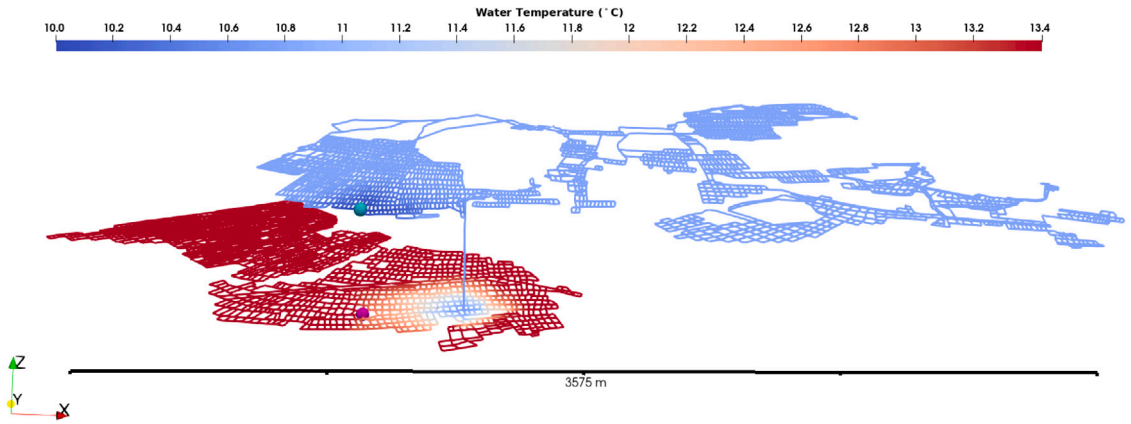

Fig. 4. Temperature distribution inside the mine workings for the Van Mildert Scenario 1 after 30 years. Water is re-injected at 10 °C at the cyan sphere and abstracted at the magenta sphere. The system flow rate at the wells is about 6.5 l/s. Vertical exaggeration x5.

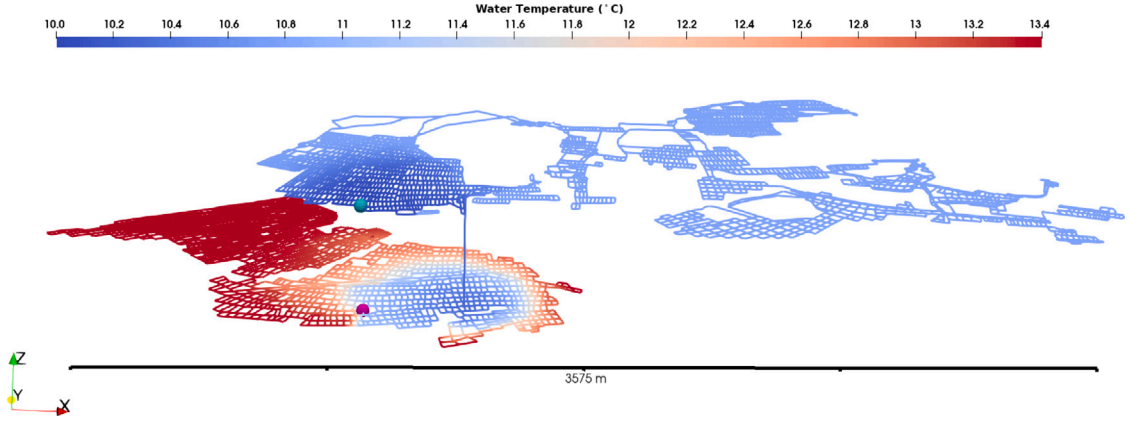

Fig. 5. Temperature distribution inside the mine workings for the Van Mildert Scenario 2 after 30 years. Water is re-injected at 10 °C at the cyan sphere and abstracted at the magenta sphere. The system flow rate at the wells is about 73.5 l/s. Vertical exaggeration x5.

the deeper seam as well. This illustrates how *GEMSToolbox* can be use to investigate the impact of different operational parameters on the subsurface mine system fast and efficiently.

3.2. Effect of rock thermal properties on abstraction temperature

Thermal conductivity and heat capacity of the material in the mines are varied to assess the importance of choosing those parameters correctly. The default values are changed to those more appropriate for sandstone and shale (see Table 1). Fig. 6 shows that the variations in thermal conductivity of the rock surrounding the mine has a greater impact on the abstraction temperature than the rock's specific heat capacity. The lower the specific heat or thermal conductivity of the rock the lower the abstraction temperature of the water will be. The deviation in abstraction temperature from the base case of scenario 1 increases over time.

3.3. Effect of flow rate on abstraction temperature

The difference between scenarios 1 and 2 is quantified by plotting the effect of flow rates against time. Fig. 7 shows the abstraction temperatures for both scenarios. The results show that the system cools over time. That the initial temperature of the abstraction water is equal to the initial rock temperature in the deeper seam. It shows that in Scenario 1, where the annual total heat demand is spread evenly over the year then the system stabilises at an abstraction temperature of 12.7 °C.

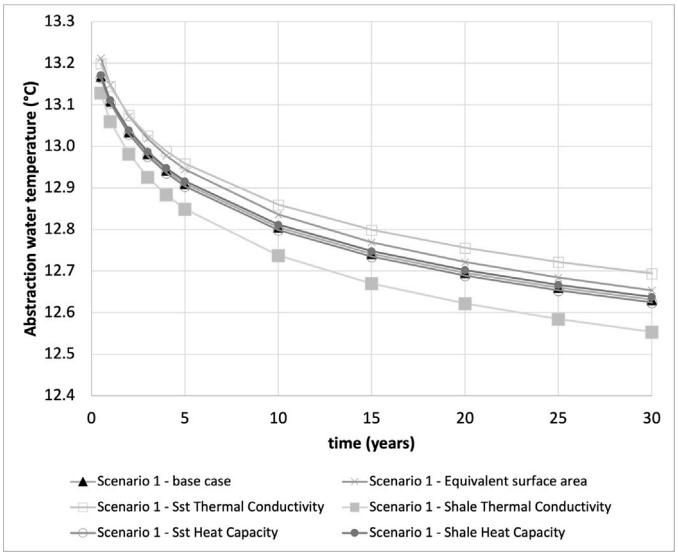

Fig. 6. Abstraction temperature of the system through time for scenario 1 with different thermal rock properties for model Scenario 1. Values measured through time at the abstraction ('magenta') points in Figs. 4 and 5. This scenario is varied by using both sandstone and shale thermal properties. These two lithologies constitute the roof and floor of the mine. The abstraction seam's starting rock temperature is 13.44 °C and the re-injection temperature is 10.00 °C.

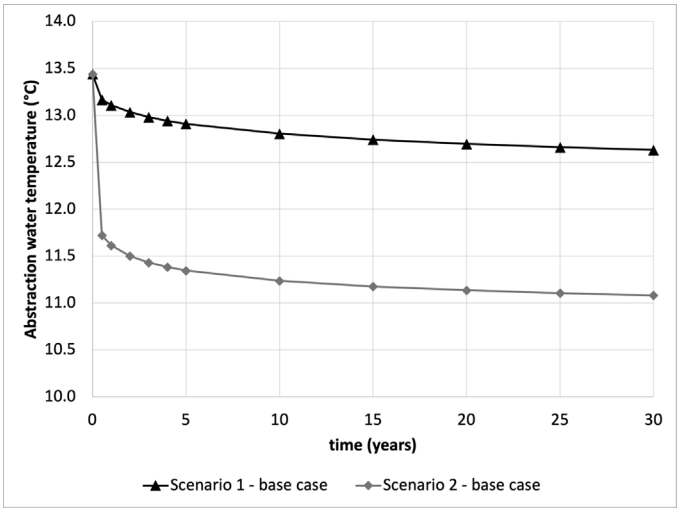

Fig. 7. Abstraction temperature of the system through time for each of the two scenarios modelled. Values measured through time at the cyan points in Figs. 4 and 5. Scenario 1 assumes the annual heat demand is equally spread out over the entire year, scenario 2 assumes that the peak demand which occurs less than 10% of the year actually occurs all year round. The abstraction seam's in-situ temperature is 13.44 °C and the re-injection temperature is 10.00 °C.

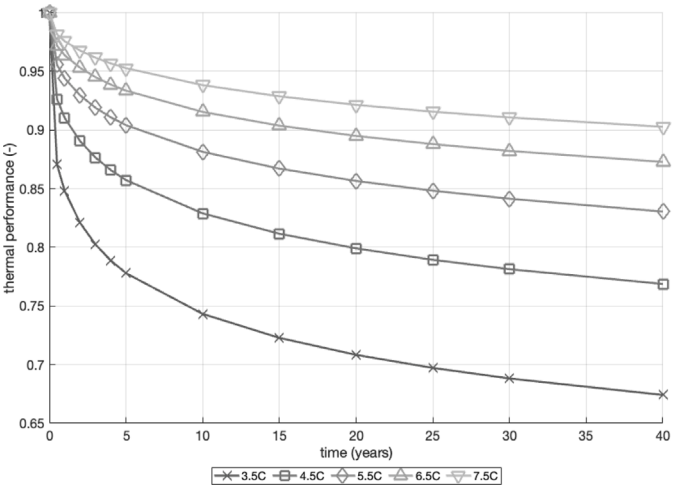

Fig. 8. Thermal performance of the system through time for variations of the first scenario. Each curve represents the Scenario 1 being ran for different changes in temperature across the heat exchanger of the heat pump, combined to the matching change in flow rate to ensure the same amount of heat is extracted from the water. In effect, for lower ΔT the flow rate is increased, whilst for higher ΔT the flow rate is decreased, to extract the required heat from the mine water.

The results also show that in the second scenario where the peak demand is used to calculate the abstraction flow rate applied over the whole year, the abstraction temperature of the system is greatly affected, and stabilises around 11.2 °C.

3.4. Effect of balancing re-injection temperature and flow rate on thermal performance

Fig. 8 illustrates how different operational parameters of the system, the flow rate and temperature drop across the heat pump's heat exchanger, affect the heat extraction from the mine water. It illustrates that increasing the temperature drop across the heat exchanger, and reducing the flow rate, increases the thermal performance of the system and reduces its drop over time when the site is operated at a constant flow rate. Such operation might be imposed by regulations or permits. The figure also shows that the greatest drop in thermal performance occurs at the start of the scheme's operation.

4. Discussion

GEMSToolbox is a novel tool to explore the feasibility of mine workings for geothermal heat extraction. Results on a hypothetical case study for the Van Mildert college illustrates some of the capabilities of the tool. This section discusses how the tool can be used to explore how the uncertainty in the subsurface propagates into uncertainty on the thermal performance of the mine system as a source of low-carbon heat. Then are discussed additional processes that should be considered in subsequent phases of the project or jointly with the thermal performance assessment undertaken using the *GEMSToolbox*.

4.1. Van Mildert college Durham University case study

This study of the feasibility of using a local mine-water heating scheme to heat the Durham University Van Mildert College residential halls is hypothetical in nature. Yet, it serves to illustrate various valuable outputs, limitations, and applications of *GEMSToolbox*.

First, It should be noted that in that particular study the two heating demand scenarios reflect two end members. The first is most realistic because it does not over inflate the total amount of heat extracted from the system each year. From an energy balance perspective it is therefore more valuable in assessing the sustainability of the scheme. It is worth noting that, in reality, and for actual costings to be meaningful, the peak load should be considered, so that the power output of the heat pump can meet peak load demand which occurs only a fraction of the year. The second scenario, can be construed as a high-end member illustrating the maximum rate of heat depletion which should be anticipated.

The drop in the thermal performance of the system (Fig. 8) indicates that the system's abstraction temperature gradually decreases over time whilst the re-injection temperature is maintained. Due to the open nature of the system the flow tends to spread around the injection and abstraction borehole increasing the sweep of the system in those areas. The rate of decline in the mine water temperature reduces gradually over time as heat is mobilised from a greater distance around the mine. In other words, the temperature difference between the mine wall and the rock is reduced over time as the rock surrounding the mine cools. From an operational perspective the drop in abstraction temperature is mostly felt in the first few years of operation. In both scenarios the temperature drop in abstraction temperature from 5 to 30 years was of less than 0.5 °C.

If it is assumed that the operational flow rates are restricted at a permitting stage, then it can be seen how *GEMSToolbox* can be used to evaluate the over sizing of the system. First, it can help predict the temperature drop over time at the abstraction point. Second, it can be used to design a system which operates at a constant flow rate but for which the temperature drop at any point during the lifetime of the project does not make the scheme economically unviable.

One point to discuss at this stage is the importance of expert knowledge in interpreting mine abandonment plans. For example, in the case study presented here, the mine shaft connecting the Hutton Seam to the Busty Seam at 1°34′36″W, 54°45′46″N was identified by a former mining engineer. This is an important consideration as these interpretations have a strong control on the results. It can therefore be said that in countries like the UK, where most of the schemes would have to be developed in disused mines using legacy data and knowledge, the new generation of engineers trained with renewable technologies would have to work hand in hand with former experts in order to assess the sites. This has strong social and timing implications for the uptake of the technology in regions where legacy mines are found.

The assignment of thermal properties to the rock mass should also be discussed. The model currently allows the user to specify a single thermal conductivity, heat capacity and density value for the rocks surrounding the mine. Due to the sequential nature of the deposits which led to the coal formations it is common for the floor of the mines to be different from the roof strata. In the represented case study the floor of the seams are shale and the roof sandstones. It has been shown that the thermal conductivity of the surrounding rock has a greater impact on the abstraction temperature than the specific heat capacity of the rock. This is explained by the fact that the water efficiently cools the rock immediately in the vicinity of the galleries and that the primary control becomes the speed at which heat can be mobilised from further within the rock. This is primarily controlled by the thermal conductivity of the rock. However, it has also been demonstrated that variation in rock thermal properties in this case study have less of an impact on the abstraction temperature than the flow rate has.

GEMSToolbox models mine galleries as cylindrical pipes as an approximation of the more complex shape of the real mine galleries. Rodríguez and Díaz [30] justify this approach, and in Appendix C the minimal difference in heat exchange between cylindrical and rectangular galleries, provided the surface area of the two galleries are the same, is illustrated. In this context, it is noted that finding the typical gallery dimensions within the mine workings is not trivial. The calculation of the representative width of the mine galleries is achieved using the 'Measure' tool in ArcGIS Pro, through which the widths of a random sample set of individual galleries was measured. Based on a population size of 10,581 pipes across the two mapped seams, a 95% confidence level, and a 5% margin of error, the determined sample size was 371. From this sample set, the average gallery width was determined to be 3.31 m. An average seam thickness (i.e. gallery height) was assumed to be 1.20 m based on discussions with former mining engineers. This average gallery width and height yields a cross-sectional area of 3.97 m. This results in an assigned pipe diameter of 2.25 m to the galleries in the model, which yield an equivalent cross-sectional area. The velocity of the water through the system is a critical control on the turbulence of the flow and hence the heat transfer coefficient applied between the rock and the water. However, the heat exchange between the rock mass and the mine water depends on the surface area of the galleries. Therefore, it might be worth considering modelling scenarios where the radius of the galleries is determined to yield an equivalent surface area to those estimated from the mine plans.

It should also be noted that the digitisation process could be improved by using AI for converting raster images of the legacy mine plans into networks which can be used in *GEMSToolbox*.

4.2. Additional modelling considerations

Here additional project considerations that will need to be evaluated during subsequent stages of the project are discussed. Usually when the initial feasibility study has been completed.

While the heat exchange models were mostly followed according to Rodríguez and Díaz [30] and Pruess and Bodvarsson [39], a few important improvements were added. Firstly, the improved heat transfer coefficient models from [38] were adopted. This reduces the overestimate in heat exchange, as very large mine systems might result in slow, laminar flow rates far away from the injection wells. Perhaps the most substantial improvement implemented in the heat exchange model is the introduction of the weighting coefficient η to interpolate between planar and radial heat transport models in a control volume defined by the closest distance to its closest neighbouring pipes. This approach ensures that in densely excavated seams, the thermal interference between neighbouring galleries is properly accounted for. The approach assumes that water flow rates of neighbouring galleries are similar, so that the 'control volume' around each gallery is equally split between the galleries. Although unlikely, it might be possible that flow velocity between neighbouring galleries differs significantly, in which case the concept of an equal split of the rock mass between the gallery control volumes needs to be revised, as most of the heat extraction will be achieved by the gallery with the faster flow, and this gallery should be assigned a larger control volume. One approach would be to ignore galleries with significantly lower flow rates when determining the distance to neighbouring galleries. The geothermal heat extraction estimate is therefore conservative, as assigning a larger control volume to the most contributing galleries will increase the total yield of the system.

The *GEMSToolbox* approach only considers open galleries, but is less well suited to account for areas where a significant proportion of galleries have been backfilled with mining waste. These regions would be better represented by porous media flow. Equally, the geometrical assumption of a pipe network breaks down when attempting to model areas mined using total extraction methods like longwall mining. Indeed, these areas resulted in entire areas of a coal seam being removed and resulting in a porous rubble forming with a fractured ceiling. One approach would be to couple the pipe network with a porous Darcian flow model of 2D elements. This approach has been demonstrated for a single goaf panel by Wu and Luo [43], but would need extending for a full mine system. We plan to address these limitations in our subsequent research.

GEMSToolbox does not provide a user friendly way to simulate the interaction with regional groundwater. Although this is technically possible by applying a source term at each node in the model to simulate the inflow and outflow of groundwater into the mine system, it is impractical to do so as it would require using the well setting keyword in the input file. The presence of a mine can potentially affect regional gradients by establishing a virtually constant hydraulic head zone relative to that regional gradient. The method employed in this research does not incorporate the heat recharge phenomenon occurring in the rock mass due to groundwater interaction, and only the heat from the rock itself is accounted for. If a substantial inflow of groundwater from the surrounding country rock is present within the mine, the cooling rate of the country rock is expected to be slower as it undergoes re-heating from the warm groundwater.

The amount of memory required to compute the flow fields require matrices of size nn^2 this can quickly reach the total memory available on most laptop or desktop systems. For a computer with about 16 GB of RAM, the total number of pipes which can be modelled in a square grid is around 24,000 depending on background processes and operating system requirements. Further work could look to implement domain decomposition techniques such as the one proposed by Diao et al. [44] to reduce memory costs and allow sequential computation of the flow field. However, it is worth noting that the approach presented here has been successfully tested on extensive mine working data with some models encompassing 4 seams and thousands of square meters (not presented here due to disclosure agreements).

At the moment, *GEMSToolbox* does not yet consider mine water reactive geochemical effects. The chemistry of the mine water is implicitly accounted for by allowing the user to specify the thermal and flow properties of the fluid. However, the geochemical interactions between the rock and the water as a consequence of the mine water scheme operations are not modelled. More accurate modelling could be used to estimate the chemical exchanges between the rock and the water based on the initial composition of the rock and the water, and the flow rate and temperature of the water. Surface treatment prior to re-injection would have to be factored in. This is an important consideration as galleries are open and ventilated during mining operations. This allows secondary minerals to form on the exposed surfaces within the mine. When activity and pumping cease, the rising groundwater dissolves these minerals, resulting in increased concentrations of iron, sulphates, and other contaminants. It is argued that the impact of reactive geochemical processes can be greatly minimised, but not fully removed, by taking a few steps. First, avoiding exposure of the mine water to oxygen (i.e. air) by ensuring the system above the water table is leak

free [15]. Second, by re-injecting the mine water back into the mine. This removes the need for stringent treatment of the water at the surface before its disposal in streams and rivers.

Erosion can lead to the instability of the mine working. This can be exacerbated during a mine water scheme if the flow rate is excessive [45]. Therefore, the risk can be reduced by minimising the velocity of the water inside the mine by targeting large open galleries and roadways to provide greater connectivity and cross sectional flow area. *GEMSToolbox* does not provide a quantitative evaluation of the magnitude of potential erosion in the workings but it does evaluate where turbulent flow might be likely, and provide insight on where to focus further investigations. Future work could look to add a module to estimate the stress on coal pillars and estimate the amount of erosion that would be required to lead to a substantial weakening of the pillars.

As reported by others [20] the sustainable use of mine water geothermal resources is contingent on its correct management. Currently, time dependent heat storage is not implemented in the code as the faster computation rates achieved rely on analytical solutions assuming a constant rate of water injection at a constant temperature. Alternative avenues to include time dependent boundary conditions compatible with the approach taken in *GEMSToolbox* are being explored as part of ongoing research, for example developing surrogate models using AI. These models could take in parameters such as the amplitude and frequency of the storage cycles. However, *GEMSToolbox* can already model continuous heat injection. For example, waste heat from an industrial user.

It is recommended that *GEMSToolbox* be integrated into initial feasibility studies workflows. Over time, as the project develops and large volumes of monitoring data become available, the development of more conventional fully 3D models could provide a more detailed evolution of the mine geothermal system to support the project at a more mature stage.

Despite the potential limitations listed in this section, *GEMSToolbox* can make a very valuable contribution on the assessment of mine water geothermal schemes at the feasibility stage by providing a platform to maximise the value of the limited data available and quickly iterate on multiple scenarios to explore uncertainty and narrow down project risk.

5. Conclusion

A significant contribution to the mine water modelling literature has been made with the presentation of *GEMSToolbox*, a novel tool to support feasibility investigation in the deployment and application of mine water as a low-carbon, local, heat source. The tool is developed to be fast and able to conduct sensitivity analyses of sufficiently large mine systems on a mid range laptop or desktop, with individual simulations taking in the order of 25 s for the example modelled in this study. *GEMSToolbox* offers an intermediate modelling approach particularly well suited to exploit the limited information available at a feasibility stage, namely legacy data including abandonment plans, and potentially more recent pumping data or temperature samples. The approach also accounts for the thermal interference between neighbouring galleries hence reducing overestimation in the abstraction temperature. *GEMSToolbox* can also be used to inform these larger modelling efforts by allowing the user to identify and isolate critical parameters of the system.

The use of *GEMSToolbox* has been demonstrated on a hypothetical case that seeks to provide mine water geothermal heat to the accommodation buildings of Van Mildert College, Durham University. In this example, it is shown that the drop in abstraction temperature of the system is mostly felt in the first 5 years of operation. It is observed that the thermal conductivity of the surrounding rocks has a greater impact on the abstraction temperature change than the specific heat capacity of those rocks. It is also indicated that the primary control on abstraction temperature in the simulations appears to be the operational wells flow rate. The conceptual limitations of the model have been discussed in relation to wider uncertainties and aims, to clearly define its scope of applicability, and to identify areas where alternative modelling approaches could be more appropriate.

Finally, some future improvements to the tool are recommended: the inclusion of porous media flow in back filled galleries and long-walled mined panels; the inclusion of fluctuating injection temperature and flow rates to allow for a fast approximation of seasonal storage solutions; AI could be used to speed up the digitisation of legacy mine plans; the segmentation of the domain could be useful to allow larger models to run, although this has not proved a limitation yet.

GEMSToolbox has the potential to make a significant contribution to the growth of MWGH as a technology by supporting the stakeholders researching and undertaking MWGH projects, by offering a solution compatible with existing feasibility workflows and computing resources available to the stakeholders driving forwards the technology.

CRediT authorship contribution statement

Julien Mouli-Castillo: Writing – review & editing, Writing – original draft, Visualization, Validation, Software, Resources, Methodology, Investigation, Formal analysis. **Jeroen van Hunen:** Writing – review & editing, Writing – original draft, Software, Resources, Project administration, Methodology, Funding acquisition, Formal analysis, Conceptualization. **Michael MacKenzie:** Writing – review & editing, Software, Methodology, Formal analysis, Data curation. **Thomas Sear:** Writing – review & editing, Validation, Software. **Charlotte Adams:** Writing – review & editing, Validation, Methodology, Conceptualization.

Declaration of competing interest

The authors declare the following financial interests/personal relationships which may be considered as potential competing interests: Jeroen van-Hunen reports financial support was provided by Engineering and Physical Sciences Research Council.

Data availability

The GEMSToolbox code is available at https://github.com/JulienMC/GEMSToolbox_v1/tree/main.Due to licensing restriction the shapeflies for the case study cannot be shared directly. However, we were advised that for academic use, the The Coal Authority (permissions@coal.gov.uk) can be contacted requesting a free academic license. The Coal Authority will then put us in contact and we will be able to share the shapefiles used.

Declaration of Generative AI and AI-assisted technologies in the writing process

During the preparation of this work the author(s) used Claude 2 in order to suggest short highlights and title which were reviewed and edited by JMC. ChatGPT was used to enhance the function headers of some of the code's functions. After using this tool/service, the author(s) reviewed and edited the content as needed and take(s) full responsibility for the content of the publication.

Acknowledgements

We thank our collaborators on the GEMS project for their insights and discussions around mine water heating. We thank the Durham Energy Institute for offering a platform to discuss our research. This research was funded by the EPSRC, United Kingdom grant number EP/V042564/1 Geothermal Energy from Mines and Solar-Geothermal heat (GEMS). For the purpose of open access, the authors have applied a Creative Commons Attribution (CC BY) licence to any Author Accepted Manuscript version arising.

Appendix A. Supplementary data

Supplementary material related to this article can be found online at https://doi.org/10.1016/j.apenergy.2024.122786.

References

[1] Friedlingstein P, O'Sullivan M, Jones MW, Andrew RM, Gregor L, Hauck J, et al. Global carbon budget 2022. Earth Syst. Sci. Data 2022;14:4811–900.
[2] UKParliament. Constituency data: Central heating, 2021 census. 2021, https://commonslibrary.parliament.uk/constituency-data-central-heating-2021-census/#:~:text=Most%20households%20in%20England%20and,1%25%20had%20no%20central%20heating.
[3] Gluyas JG, Adams CA, Wilson IA. The theoretical potential for large-scale underground thermal energy storage (UTES) within the UK. Energy Rep 2020;6:229–37.
[4] BEIS. Inland consumption of primary fuels and equivalents for energy use. 2022, Digest of the UK Energy Statistics Table 1.1.1.
[5] BEIS. Supply and consumption of natural gas and colliery methane. 2022, Digest of UK Energy Statistics 4.2.
[6] DESNZ. Provisional UK greenhouse gas emissions national statistics. 2022.
[7] BEIS. Net zero strategy: Build back greener. 2021, p. 368,
[8] Kirkup B, Cavey A, Lawrence D, Crane M, Gluyas J, Handley W. The case for mine energy-unlocking deployment at scale in the UK. 2021.
[9] Farr G, Busby J, Wyatt L, Crooks J, Schofield DI, Holden A. The temperature of britain's coalfields. Quarterly J. Eng. Geol. Hydrogeol. 2020;54(3).
[10] Adams C, Gluyas J. Mining for heat. Geoscientist 2019;29:10–5.
[11] Al-Habaibeh A, Athresh AP, Parker K. Performance analysis of using mine water from an abandoned coal mine for heating of buildings using an open loop based single shaft GSHP system. Appl Energy 2018;211:393–402.
[12] Zhao Y, Liu L, Wen D, Zhang B, Zhang X, Huan C, et al. Experimental study of horizontal ground heat exchangers embedded in the backfilled mine stopes. Geothermics 2022;100:102344.
[13] Liu H, Rodriguez-Dono A, Zhang J, Zhou N, Wang Y, Sun Q, et al. A new method for exploiting mine geothermal energy by using functional cemented paste backfill material for phase change heat storage: Design and experimental study. J Energy Storage 2022;54(March):105292.
[14] Liu H, Zhang J, Rodriguez-Dono A, Zhou N, Wang Y, Sun Q, et al. Utilization of mine waste heat in phase change rechargeable battery. Appl Therm Eng 2023;233(July):121136.
[15] Banks D, Athresh A, Al-Habaibeh A, Burnside N. Water from abandoned mines as a heat source: Practical experiences of open- and closed-loop strategies, United Kingdom. Sustain. Water Resour. Manag. 2017;5:29–50.
[16] Walls DB, Banks D, Peshkur T, Boyce AJ, Burnside NM. Heat recovery potential and hydrochemistry of mine water discharges from Scotland's coalfields. Earth Sci. Syst. Soc. 2022;2.
[17] Walls DB, Banks D, Boyce AJ, Burnside NM. A review of the performance of minewater heating and cooling systems. Energies 2021;14:1–33.
[18] Ferket HLW, Laenen BJM, Tongeren PCHV. Transforming flooded coal mines to large-scale geothermal and heat storage reservoirs: What can we expect? IMWA Mine Water - Manag. Chall. 2011;171–6.
[19] Silva JP, McDermott C, Fraser-Harris A. The value of a hole in coal: Assessment of seasonal thermal energy storage and recovery in flooded coal mines. Earth Sci. Syst. Soc. 2022;2.
[20] Fraser-Harris A, McDermott CI, Receveur M, Mouli-Castillo J, Todd F, Cartwright-Taylor A, et al. The geobattery concept: A geothermal circular heat network for the sustainable development of near surface low enthalpy geothermal energy to decarbonise heating. Earth Sci. Syst. Soc. 2022;2.
[21] Xu Y, Li Z, Chen Y, Jia M, Zhang M, Li R. Synergetic mining of geothermal energy in deep mines: An innovative method for heat hazard control. Appl Therm Eng 2022;118398.
[22] Bao T, Liu ZL. Thermohaline stratification modeling in mine water via double-diffusive convection for geothermal energy recovery from flooded mines. Appl Energy 2019;237:566–80.
[23] Loredo C, Roqueñí N, Ordóñez A. Modelling flow and heat transfer in flooded mines for geothermal energy use: A review. Int J Coal Geol 2016;164:115–22.
[24] Clauser C. Numerical simulation of reactive flow in hot aquifers: SHEMAT and processing SHEMAT. Springer Science & Business Media; 2003.
[25] Pruess K, Oldenburg C, Moridis G. Tough2 user's guide, version 2. (November 1999), 2012, p. 1–210.
[26] Kolditz O, Bauer S, Bilke L, Böttcher N, Delfs JO, Fischer T, et al. OpenGeoSys: An open-source initiative for numerical simulation of thermo-hydro-mechanical/chemical (THM/C) processes in porous media. Environ. Earth Sci. 2012;67:589–99.
[27] Thiery D, Jacquemet N, Picot-Colbeaux G, Kervevan C, Andre L, Azaroual M. Validation of Marthe-react coupled surface and groundwater reactive transport code for modeling hydro systems. In: PROCEEDINGS, TOUGH Symposium 2009. 2009, p. 1–8.
[28] Lauwerier HA. The transport of heat in oil layer caused by the injection of hot fluid. Appl. Sci. Res. 1955;5:145–55.
[29] Wang Y, Hu H, Sun X, Zhang Y, Gong D. Unified operation optimization model of integrated coal mine energy systems and its solutions based on autonomous intelligence. Appl Energy 2022;328:120106.
[30] Rodríguez R, Díaz MB. Analysis of the utilization of mine galleries as geothermal heat exchangers by means a semi-empirical prediction method. Renew Energy 2009;34:1716–25.
[31] Rossman L. Epanet 2 users manual. 2008, p. 104.
[32] Todini E, Pilati S. A gradient method for the analysis of pipe networks. In: Computer applications in water supply, vol. 1, 1988, p. 1–20.
[33] Todini E, Rossman LA. Unified framework for deriving simultaneous equation algorithms for water distribution networks. J Hydraul Eng 2013;139:511–26.
[34] Brown GO. The history of the Darcy-Weisbach equation for pipe flow resistance. In: Rogers JR, Fredrich AJ, editors. Proceedings of the Environmental and Water Resources History. American Society of Civil Engineers; 2002, p. 34–43.
[35] Swamee PK, Jain AK. Explicit equations for pipe-flow problems. J. Hydraul. Div. 1976;102:657–64.
[36] Dunlop E. WADI Users Manual. Dublin, Ireland: Local Government Computer Services Board; 1991.
[37] Gnielinski V. Neue Gleichungen für den Wärme- und den Stoffübergang in turbulent durchströmten Rohren und Kanälen. Forsch. Ing. A 1975;41:8–16.
[38] Loredo C, Banks D, Roqueñí N. Evaluation of analytical models for heat transfer in mine tunnels. Geothermics 2017;69:153–64.
[39] Pruess K, Bodvarsson G. Thermal effects of reinjection in geothermal reservoirs with major vertical fractures. In: San Francisco, CA, October 5-8, Society of Petroleum Engineers 58th Annual Technical Conference and Exhibition 1983. 1984, p. 1567–78.
[40] MacKenzie M. Modelling mine energy systems: A feasibility study of the implementation of a minewater heating system on the university estate. 2022.
[41] Banks D, Steven J, Black A, Naismith J. Conceptual modelling of two large-scale mine water geothermal energy schemes: Felling, Gateshead, UK. Int J Environ Res Public Health 2022;19.
[42] Verhoeven R, Willems E, Harcouët-Menou V, Boever ED, Hiddes L, t. Veld PO, et al. Minewater 2.0 project in Heerlen the Netherlands: Transformation of a geothermal mine water pilot project into a full scale hybrid sustainable energy infrastructure for heating and cooling. Energy Procedia 2014;46:58–67.
[43] Wu F, Luo Y. An innovative finite tube method for coupling of mine ventilation network and gob flow field: Methodology and application in risk analysis. Min. Metall. Explor. 2020;(37):1517–30.
[44] Diao K, Wang Z, Burger G, Chen CH, Rauch W, Zhou Y. Speedup of water distribution simulation by domain decomposition. Environ. Model. Softw. 2014;52:253–63.
[45] Sizer KE, Gill M. Pillar failure in shallow coal mines—a recent case history. Min. Technol. 2000;109:146–52.